Inorganic Chemistry

Article

pubs.acs.org/IC

Vapochromic and Mechanochromic Phosphorescence Materials Based on a Platinum(II) Complex with 4-Trifluoromethylphenylacetylide

Xu Zhang,[†] Jin-Yun Wang,[†] Jun Ni,[†] Li-Yi Zhang,[†] and Zhong-Ning Chen*[,†,‡]

[†]State Key Laboratory of Structural Chemistry, Fujian Institute of Research on the Structure of Matter, Chinese Academy of Sciences, Fuzhou, Fujian 350002, China

[‡]State Key Laboratory of Organometallic Chemistry, Shanghai Institute of Organic Chemistry, Chinese Academy of Sciences, Shanghai 200032, China

Supporting Information

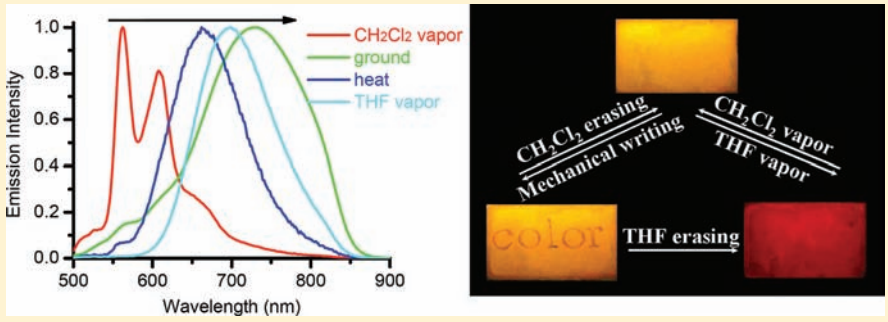

ABSTRACT: Planar platinum(II) complex $Pt(Me_3SiC{\equiv}CbpyC{\equiv}CSiMe_3)(C{\equiv}CC_6H_4CF_3\text{-}4)_2$ (**6**) with 5,5′-bis-(trimethylsilylethynyl)-2,2′-bipyridine and 4-trifluoromethylphenylacetylide exhibits remarkable luminescence vapochromic and mechanochromic properties and a thermo-triggered luminescence change. Solid-state **6** is selectively sensitive to vapors of oxygen-containing volatile compounds such as tetrahydrofuran (THF), dioxane, and tetrahydropyrane (THP) with phosphorescence vapochromic response red shifts from 561 and 608 nm to 698 nm (THF), 689 nm (dioxane), and 715 nm (THP), respectively. Upon being mechanically ground, desolvated **6**, **6**·CH_2Cl_2, and **6**·$^1/_2CH_2ClCH_2Cl$ exhibit significant mechanoluminescence red shifts from 561 and 608 nm to 730 nm, while vapochromic crystalline species **6**·THF, **6**·dioxane, or **6**·THP affords a mechanoluminescence blue shift from 698 nm (THF), 689 nm (dioxane), or 715 nm (THP) to 645 nm, respectively. When the compounds are heated, a thermo-triggered luminescence change occurs, in which bright yellow luminescence at 561 and 608 nm turns to red luminescence at 667 nm with a drastic red shift. The multi-stimulus-responsive luminescence switches have been monitored by the changes in emission spectra and X-ray diffraction patterns. Both X-ray crystallographic and density functional theory studies suggest that the variation in the intermolecular Pt−Pt interaction is the key factor in inducing an intriguing luminescence switch.

INTRODUCTION

It has been demonstrated that square-planar Pt(diimine)$(C{\equiv}CR)_2$ (R = alkyl or aryl) complexes usually exhibit bright luminescence at ambient temperature, originating mostly from $^3[d\pi(Pt) \rightarrow \pi^*(diimine)]/^3[d\pi(C{\equiv}CR) \rightarrow \pi^*(diimine)]$ $^3MLCT/^3LLCT$ triplet excited states.[1−5] These planar molecules favor formation of aggregate species through intermolecular Pt−Pt and $\pi-\pi$ interactions that are highly sensitive to external stimuli such as solvate, heat, and mechanical force, triggering intriguing color and luminescence changes.[6−8] Such stimulus-responsive luminescence switches have extensive applications in sensing, optical recording, memory, and display. Among various luminescence and color changes in response to external stimuli, luminescence vapochromism,[6−27] mechanochromism,[7c,d,22a,b,23,28−36] and thermochromism[32,37−42] occur frequently in solid-state materials based on various metal coordination compounds. External stimuli cause variations in metallophilic contact, $\pi-\pi$ stacking, H-bonding interaction, or metal−solvent bonding, thus resulting in an increase or decrease in the ^3MLCT or ^3LLCT energy level, respectively, which is responsible for the blue or red shift, respectively, of the phosphorescent emission.

We have been interested in the stimulus-responsive phosphorescence switch in square-planar bis(σ-acetylide) platinum(II) complexes with 5,5′-bis(trimethylsilylethynyl)-2,2′-bipyridine ($Me_3SiC{\equiv}CbpyC{\equiv}CSiMe_3$) or 5-(trimethylsilylethynyl)-2,2′-bipyridine ($Me_3SiC{\equiv}Cbpy$).[7] These planar platinum(II) complexes exhibit remarkable luminescence vapochromic or/and mechanochromic properties, inducing

Received: November 10, 2011
Published: May 2, 2012

   dx.doi.org/10.1021/ic202421d | *Inorg. Chem.* 2012, 51, 5569−5579

Table 1. Crystallographic Data for 6·CH_2Cl_2, 6·$^1/_2CH_2ClCH_2Cl$, and 6·THF

	6·CH_2Cl_2	6·$^1/_2CH_2ClCH_2Cl$	6·THF
empirical formula	$C_{39}H_{34}Cl_2F_6N_2PtSi_2$	$C_{39}H_{34}ClF_6N_2PtSi_2$	$C_{42}H_{40}F_6N_2OPtSi_2$
formula weight	966.85	931.39	954.03
crystal system	monoclinic	monoclinic	monoclinic
space group	$P2_1/c$	$P2_1/c$	$C2/c$
a (Å)	7.1353(7)	7.084(3)	17.388(7)
b (Å)	38.393(3)	37.329(17)	39.549(15)
c (Å)	15.2803(17)	15.811(7)	13.504(6)
β (deg)	96.035(7)	94.648(7)	105.179(8)
V (Å^3)	4162.8(7)	4168(3)	8963(6)
Z	4	4	8
ρ_{calcd} (g/cm^{-3})	1.543	1.485	1.414
μ (mm^{-1})	3.612	3.544	3.241
radiation (λ, Å)	0.71073	0.71073	0.71073
temp (K)	293(2)	293(2)	293(2)
R1(F_o)^a	0.0474	0.0691	0.0733
wR2(F_o^2)^b	0.1701	0.2116	0.2118
GOF	1.020	1.070	1.035

^{a}R1 = $\sum|F_o - F_c|/\sum F_o$. $^b w\text{R2} = \sum[w(F_o^2 - F_c^2)^2]/\sum[w(F_o^2)]^{1/2}$.

significant emission shifts in response to vapors of specific volatile organic compounds (VOCs) or mechanical grinding. Aiming at increasing the contrast of stimulus-responsive luminescence color changes as well as exploring the influence of various substituents on crystal packing and luminescence conversion in response to external stimuli, we found a feasible approach is to increase the ^{3}MLCT/^{3}LLCT level by introducing electron-donating substituents into $Me_3SiC{\equiv}CbpyC{\equiv}CSiMe_3$ or electron-withdrawing substituents into phenylacetylide. Considering that introduction of an electron-withdrawing CF_3 group onto phenylacetylide ($C{\equiv}CC_6H_4R$) would lower the HOMO level and increase the ^{3}MLCT/^{3}LLCT energy, Pt($Me_3SiC{\equiv}CbpyC{\equiv}C$-$SiMe_3$)-($C{\equiv}CC_6H_4CF_3$-4)$_2$ (**6**) was synthesized to produce blue-shifted phosphorescent emission (568 and 608sh nm in CH_2Cl_2) relative to that of Pt($Me_3SiC{\equiv}CbpyC{\equiv}C$-$SiMe_3$)-($C{\equiv}CC_6H_5$)$_2$ (**2**; λ_{em} = 616 nm in CH_2Cl_2). It is found that phosphorescent emission in solid materials based on complex **6** is highly sensitive to vapors of some O-heterocyclic VOCs, heating, and mechanical grinding with multi-stimulus-responsive luminescence switches. In contrast with Pt($Me_3SiC{\equiv}CbpyC{\equiv}CSiMe_3$)($C{\equiv}CC_6H_5$)$_2$ (**1**)[7b] that exhibits luminescence vapochromism to vapors of three halocarbons such as CH_2Cl_2, $CHCl_3$, and CH_3I with drastic vapochromic red shift responses, complex **6** is selectively sensitive to vapors of three O-heterocyclic VOCs with drastic vapochromic red shift responses from 561 and 608 nm to 698 nm (THF = tetrahydrofuran), 689 nm (dioxane), or 715 nm (THP = tetrahydropyrane). Furthermore, unusual blue-shifted or red-shifted mechanochromic luminescence is exhibited for the **6**·VOC complex depending on the solvate VOC, in which the **6**·THF complex displays obviously blue-shifted luminescence in response to mechanical grinding whereas desolvated **6**, **6**·CH_2Cl_2, and **6**·$^1/_2CH_2ClCH_2Cl$ afford remarkably red-shifted mechanochromic luminescence.

EXPERIMENTAL SECTION

General Procedures and Materials. All operations were conducted under a dry argon atmosphere using Schlenk techniques and vacuum-line systems unless otherwise specified. The solvents were dried, distilled, and degassed prior to use except that those for spectroscopic measurements were of spectroscopic grade. 5,5′-Bis(trimethylsilylethynyl)-2,2′-bipyridine ($Me_3SiC{\equiv}CbpyC{\equiv}CSiMe_3$), 1-ethynyl-4-(trifluoromethyl)benzene ($HC{\equiv}CC_6H_4CF_3$-4), and Pt($Me_3SiC{\equiv}CbpyC{\equiv}CSiMe_3$)$Cl_2$ were prepared by synthetic procedures described in the literature.[7,43] Other reagents were purchased from commercial sources and used as received unless specified otherwise.

Pt($Me_3SiC{\equiv}CbpyC{\equiv}CSiMe_3$)($C{\equiv}CC_6H_4CF_3$-4)$_2$ (6). To a dichloromethane (50 mL) solution of 1-ethynyl-4-(trifluoromethyl)-benzene (85 mg, 0.5 mmol) were added Pt($Me_3SiC{\equiv}CbpyC{\equiv}CSiMe_3$)$Cl_2$ (123 mg, 0.20 mmol), CuI (1 mg), and diisopropylamine (2 mL) with stirring for 1 day at ambient temperature. After the solvents were removed in vacuo, the product was purified by chromatography on a silica gel column using dichloromethane as the eluent. Yield: 82% (145 mg). Anal. Calcd for desolvated $C_{38}H_{32}F_6N_2PtSi_2$: C, 51.75; H, 3.66; N, 3.18. Found: C, 51.57; H, 3.59; N, 3.29. ESI-MS: m/z 882 [M + H]$^+$. ^{1}H NMR ($CDCl_3$): δ 9.86 (d, 2H, J = 1.6 Hz, bpy), 8.20 (dd, 2H, J = 1.6 Hz, J = 8.4 Hz, bpy), 7.97 (d, 2H, J = 8.4 Hz, bpy), 7.57 (d, 4H, J = 8.0 Hz, C_6H_4), 7.50 (d, 4H, J = 8.4 Hz, C_6H_4), 0.28 (s, 18H, CH_3). IR (KBr disk): 2117s ($C{\equiv}CPt$), 2163m ($C{\equiv}CSiMe_3$), 1250m cm^{-1} (Si−C).

Physical Measurements. Spectroscopic measurements for unground solid samples were performed using crystalline species isolated from the solutions. The ground samples were made by mechanically grinding the crystalline species in an agate mortar. UV−vis absorption spectra in solutions were measured on a Perkin-Elmer Lambda 25 UV−vis spectrophotometer. UV−vis diffuse reflectance spectra in solid states were recorded with a Perkin-Elmer Lambda 900 UV−vis−NIR spectrophotometer. Infrared spectra (IR) were recorded on a Magna 750 FT-IR spectrophotometer with KBr pellets. Elemental analyses (C, H, N) were conducted on a Perkin-Elmer model 240 C elemental analyzer. ^{1}H NMR spectra were recorded on a Bruker Advance 400 (400 MHz) spectrometer with $SiMe_4$ as the internal reference. Electrospray ionization mass spectrometry (ESI-MS) was performed on a Finnigan LCQ mass spectrometer using dichloromethane and methanol as mobile phases. Powder X-ray diffraction (XRD) measurements were recorded on Rigaku miniflex II desktop X-ray diffractometer and Bruker D8 Advance diffractometer using Cu Kα radiation. Emission and excitation spectra were recorded on a Perkin-Elmer LS55 luminescence spectrometer with a red-sensitive photomultiplier type R928 instrument. Emission lifetimes in solid states and degassed solutions were determined on an Edinburgh analytical instrument (F900 fluorescence spectrometer) using an LED laser with excitation at 440 nm. The emission quantum yield (Φ_{em}) in a degassed dichloromethane solution at room temperature was estimated using [Ru(bpy)$_3$](PF_6)$_2$ in acetonitrile as the reference standard (Φ_{em} =

dx.doi.org/10.1021/ic202421d | Inorg. Chem. 2012, 51, 5569−5579

Scheme 1

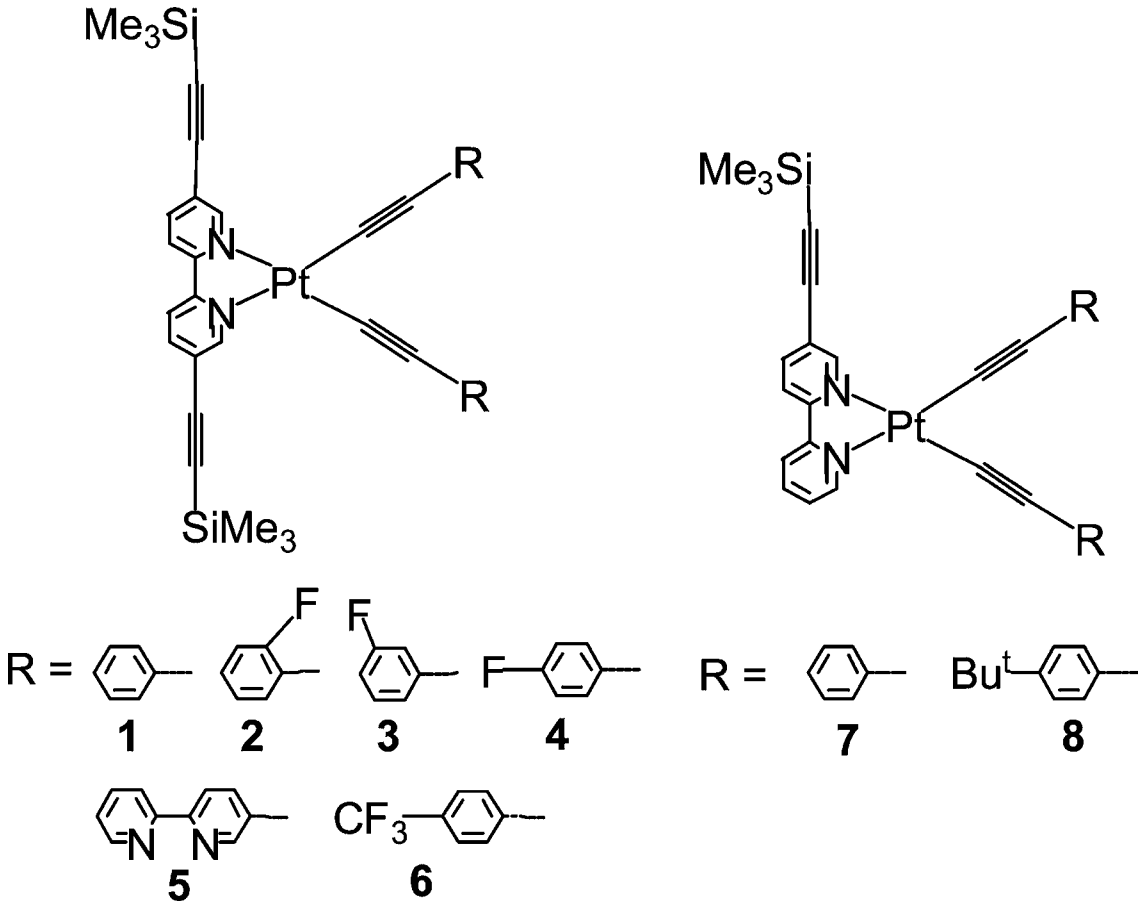

0.062).[44] To probe the selectivity and reversibility of the vapochromic properties with respect to specific VOCs, a concentrated CH_2Cl_2 solution of **6** was put on quartz disks that were purged with N_2 to dry. Luminescence vapochromic experiments were performed upon sufficient exposure of the quartz disks to various saturated VOC vapors at ambient temperature for 5−10 min. A rapid vapochromic response is usually observed in 15 s to 2 min depending on the sample thickness in quartz disks. A PMMA film of complex **6** was made on a quartz slide (2.5 cm × 4 cm) using the spin coating method, in which the solution was prepared by dissolving complex **6** (10 mg) and PMMA (polymethylmethacrylate, 40 mg) in dichloromethane (2 mL).

Determination of Crystal Structures. Single crystals of **6**·$^1/_2CH_2ClCH_2Cl$, **6**·CH_2Cl_2, and **6**·THF were obtained by layering petroleum ether onto the corresponding solutions of **6** with solvate VOCs as the solvents. Single crystals sealed in capillaries with mother liquor were measured on a Saturn 70 CCD diffractometer by the ω scan technique at room temperature using graphite-monochromated Mo Kα (λ = 0.71073 Å) radiation. CrystalClear was used for data reduction and empirical absorption correction. The structures were determined by direct methods. The heavy atoms were located with an E-map, and the rest of the non-hydrogen atoms were found in subsequent Fourier maps. All non-hydrogen atoms were refined anisotropically, while the hydrogen atoms were generated geometrically and refined with isotropic thermal parameters. The structures were refined on F^2 by full-matrix least-squares methods using *SHELXTL*-97.[45] For **6**·THF, 4-(trifluoromethylphenyl)acetylide and solvate THF exhibit a statistical distribution with two sets of corresponding identical groups. The occupancy percentage of atoms C30−C38 and F4−F6 (4-trifluoromethylphenyl) as well as O01 and C01−C04 (solvate THF) is 47.4%, whereas that of counterparts C30B−C38B and F4B−F6B (4-trifluoromethylphenyl) as well as O01B and C01B−C04B (solvate THF) is 52.6%. Crystallographic data for **6**·CH_2Cl_2, **6**·$^1/_2CH_2ClCH_2Cl$, and **6**·THF are presented in Table 1.

Theoretical Calculation Methodology. To gain insight into the electronic and spectroscopic properties as well as the nature of the origin of absorption and emission of complex **6**, time-dependent density functional theory (DFT/TD-DFT)[46−48] with the gradient-corrected correlation functional PBE1PBE[49] was employed for the calculations. First, the structural geometry of complex **6** as an isolated molecule from the solvent phase in the ground state was optimized at the DFT level of theory without symmetry constraints. To analyze the spectroscopic properties, 100 singlet and 6 triplet excited states were obtained to determine the vertical excitation energies in a dichloromethane solution by performing the TD-DFT calculations on the basis of the optimized geometrical structure. The polarized continuum model method (PCM)[50] with dichloromethane as the solvent was used to calculate all the electronic structures in solution. In these calculations, the Stuttgart−Dresden (SDD)[51] basis set consisting of the effective core potentials (ECP) was employed for the platinum(II) and silicon(IV) atoms, and the 6-31G(p,d) polarized double-ζ basis set was used for the remaining atoms. To precisely describe the electronic structures, one additional *f*-type polarization function was implemented for the platinum(II) atom (α_f = 0.18).[52]

To compare transition characteristics that contribute to the absorption and emission spectra in crystalline species **6**·VOC with different solvate VOCs, TD-DFT calculations were performed on **6**·$^1/_2CH_2ClCH_2Cl$ and **6**·THF using a pair of symmetry-related platinum(II) moieties (dimeric model) with the shortest intermolecular Pt···Pt distance. As the solvate molecules were found to exert an insignificant influence on the calculated results, all the calculations on **6**·$^1/_2CH_2ClCH_2Cl$ and **6**·THF were performed by using a pair of symmetry-related square-planar platinum(II) moieties with the shortest intermolecular Pt···Pt distance without considering the solvate molecules. All calculations were performed with Gaussian 03.[53]

dx.doi.org/10.1021/ic202421d | *Inorg. Chem.* 2012, 51, 5569−5579

RESULTS AND DISCUSSION

Synthesis and Characterization. Complex **6** and related square-planar platinum(II) complexes are shown in Scheme 1. Crystalline species **6**·VOC were obtained from the corresponding solutions with solvate VOCs as the solvents by layering petroleum ether. The solvate VOC was identified by thermal analysis and mass spectrometry, thermogravimetric studies, and ^{1}H NMR spectra (Figures S1−S6 of the Supporting Information). The desolvated crystalline species **6** could be obtained by removal of the solvate CH_2Cl_2 or CH_2ClCH_2Cl in **6**·CH_2Cl_2 or **6**·$^1/_2CH_2ClCH_2Cl$ at ambient temperature under vacuum for several hours, which was confirmed by thermogravimetric studies (Figures S4 and S5 of the Supporting Information). Nevertheless, desolvated crystalline species **6** could not be obtained from **6**·THF, in which the solvate THF in **6**·THF could not be removed by exposure to vacuum for 2 h at ambient temperature (Figure S6 of the Supporting Information).

The crystal structures of **6**·$^1/_2CH_2ClCH_2Cl$, **6**·CH_2Cl_2, and **6**·THF were determined by X-ray crystallography. Crystal packing diagrams are depicted in Figure 1 for **6**·CH_2Cl_2 and

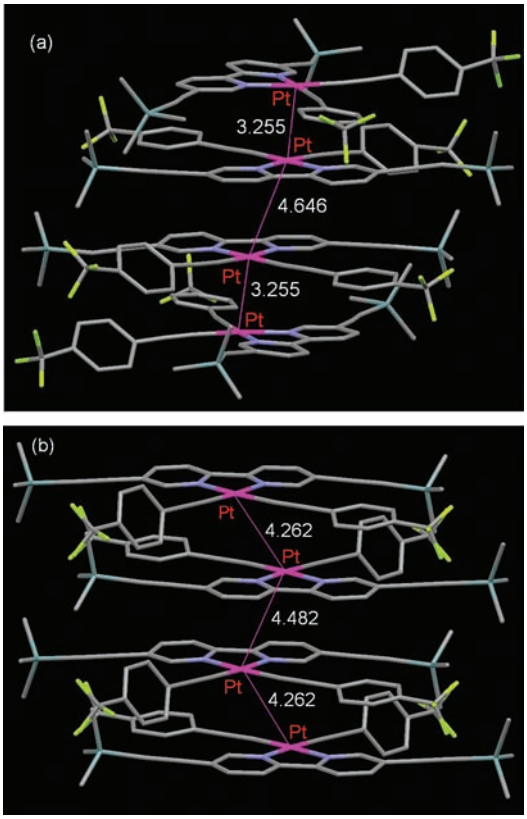

Figure 1. Packing diagrams of planar platinum(II) complexes **6**·VOC (VOC = THF or CH_2Cl_2). (a) Alternately staggered and antiparallel stacking pattern in **6**·THF with short (3.255 Å) and long (4.646 Å) Pt···Pt distances. (b) Antiparallel pattern in **6**·CH_2Cl_2 with long Pt···Pt distances (4.262 and 4.482 Å).

6·THF and Figure S9 of the Supporting Information for **6**·$^1/_2CH_2ClCH_2Cl$. The platinum(II) centers exhibit a distorted square-planar coordination environment composed of N_2C_2 donors from chelating $Me_3SiC{\equiv}CbpyC{\equiv}CSiMe_3$ and bis(σ-4-trifluoromethylphenyl)acetylide. The Pt−C [1.942(10)−1.962(11) Å] and Pt−N [2.049(8)−2.099(8) Å] lengths together with the C−Pt−N, C−Pt−C, and N−Pt−N angles are comparable to those in other Pt($Me_3SiC{\equiv}CbpyC{\equiv}CSiMe_3$)(acetylide)$_2$ complexes.[7]

Planar platinum(II) complex moieties in **6**·$^1/_2CH_2ClCH_2Cl$ (Figure S9b of the Supporting Information) and **6**·CH_2Cl_2 (Figure 1b) are packed in an antiparallel pattern with adjacent Pt···Pt distances being alternately 4.262(11) and 4.482(12) Å for the former and 4.371(10) and 4.377(10) Å for the latter. The crystal structure of **6**·THF (Figure 1a), nevertheless, exhibits an alternately staggered and anitiparallel packing pattern to afford a short Pt···Pt distance and a long Pt···Pt distance [3.255(8) and 4.646(10) Å, respectively]. It has been revealed that a staggered packing pattern favors formation of a short Pt···Pt distance (<3.5 Å) whereas an antiparallel pattern always induces a long Pt···Pt distance (>3.5 Å) for planar bis(σ-acetylide) platinum(II) complexes with functionalized 2,2′-bipyridyl ligands.[7] The shortest Pt···Pt distance in **6**·THF [3.255(8) Å] is even slightly shorter than those found in Pt($Me_3SiC{\equiv}CbpyC{\equiv}CSiMe_3$)($C{\equiv}CC_6H_5$)$_2$·$CHCl_3$ [3.302(1) Å][7b] and Pt($Me_3SiC{\equiv}CbpyC{\equiv}CSiMe_3$)($C{\equiv}CC_6H_4F$-4)$_2$·$^1/_2CH_2Cl_2$ [3.315(9) Å][7c] with a staggered packing pattern.

Host−guest interactions between solvate CH_2Cl_2 and platinum(II) moieties exist in the crystal structure of **6**·CH_2Cl_2 (Figure S10 of the Supporting Information), including the ClC-H···π(C≡C) interaction and C_6H_4···ClCH hydrogen bonds together with intermolecular F···H−C hydrogen bonds between $C{\equiv}CC_6H_4CF_3$-4 and $Me_3SiC{\equiv}CbpyC{\equiv}CSiMe_3$. For **6**·$^1/_2CH_2ClCH_2Cl$ (Figure S11 of the Supporting Information), the solvate CH_2ClCH_2Cl molecules are inserted into the channels and cavities of the crystal structures and arranged through a short Cl···Cl contact [3.381(11) Å] between neighboring CH_2ClCH_2Cl molecules. The solvate THF is associated with the platinum(II) moiety in **6**·THF (Figure S12 of the Supporting Information) through intermolecular interactions, including C−H···O(THF) and F···H−C(THF) hydrogen bonds.

Photophysical Properties. The UV−vis electronic absorption spectrum of **6** in CH_2Cl_2 exhibits high-energy absorption bands with maxima at 293, 327, and 369 nm due to mainly ligand-centered transitions together with a broad low-energy band with the maximum centered at 430 nm, which can be ascribed to dπ(Pt) → π^*($Me_3SiC{\equiv}CbpyC{\equiv}CSiMe_3$) ^{1}MLCT and π($C{\equiv}CC_6H_4CF_3$-4) → π^*($Me_3SiC{\equiv}CbpyC{\equiv}CSiMe_3$) ^{1}LLCT transitions.[7] The low-energy absorption bands are solvent-dependent, affording negative solvatochromic properties (Figure S14 of the Supporting Information), which are progressively red-shifted with a gradual decrease in solvent polarity. Upon excitation at wavelengths longer than 320 nm, complex **6** (Table 2) shows bright yellow solution luminescence with vibronic-structured emission centered at 568 (608sh) nm (Figure S13 of the Supporting Information) and the lifetime being 0.70 μs in fluid CH_2Cl_2. A significant Stokes shift together with a microsecond range of lifetimes reveals that the emission is phosphorescent in nature with a triplet excited state.[1−8] Compared with that of complex **1** (616 nm),[7b] the emission of complex **6** (568 and 608sh nm) in fluid CH_2Cl_2 is obviously blue-shifted because of the introduction of an electron-withdrawing CF_3 group onto phenylacetylide, in which the ^{3}MLCT/^{3}LLCT level is indeed increased. In comparison with unstructured solution emission in platinum(II) complexes Pt($Me_3SiC{\equiv}CbpyC{\equiv}CSiMe_3$)($C{\equiv}CR$)$_2$ (R is C_6H_5 for **1**, $C{\equiv}CC_6H_4F$-2 for **2**, $C{\equiv}CC_6H_4F$-3 for **3**, C≡

dx.doi.org/10.1021/ic202421d | Inorg. Chem. 2012, 51, 5569−5579

Table 2. Luminescence Data of 6 in CH_2Cl_2 and Solid State at Ambient Temperature

sample	sample state	λ_{em} (nm)	τ_{em} (μs)	Φ_{em} (%)
6	CH_2Cl_2	568 (608sh)	0.70	10.9
	unground	561, 608	0.95	
	ground	730	0.09	
	heated	667	0.82	
6·THF	unground	698	0.07	
	ground	645	4.07	
6·dioxane	unground	689	0.11	
	ground	647	4.53	
6·THP	unground	715	0.06	
	ground	645	3.49	

[a]The quantum yield in a degassed dichloromethane solution was estimated relative to that of $[Ru(bpy)_3](PF_6)_2$ in acetonitrile as the standard (Φ_{em} = 6.2%).

CC_6H_4F-4 for **4**, and C≡Cbpy-5 for **5**) described previously,[7] the vibronic-structured emission spectrum with vibrational progressional spacing of 1160 cm^{-1} in complex **6** is typical for the C=C and C=N stretching frequencies of the aromatic rings in $Me_3SiC{\equiv}CbpyC{\equiv}CSiMe_3$, suggesting an increased contribution from $Me_3SiC{\equiv}CbpyC{\equiv}CSiMe_3$-based phosphorescence. As revealed by DFT studies (Table S3 of the Supporting Information), the phosphorescent emission in complex **6** contains indeed a substantial contribution from the $Me_3SiC{\equiv}CbpyC{\equiv}CSiMe_3$ ($\pi \rightarrow \pi^*$) intraligand triplet excited state as a consequence of introduction of an electron-withdrawing CF_3 group onto phenylacetylide.

The solid-state UV–vis electronic spectra of crystalline species **6**·CH_2Cl_2, **6**·$^1/_2CH_2ClCH_2Cl$, and **6**·THF and their corresponding ground samples are depicted in Figure 2. On

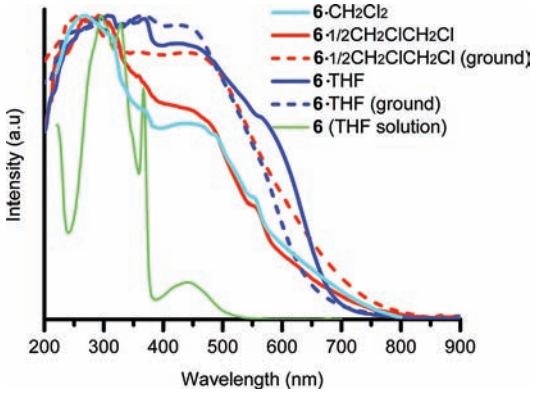

Figure 2. UV–vis electronic spectra of crystalline species (solid lines) **6**·CH_2Cl_2 (cyan), **6**·$^1/_2CH_2ClCH_2Cl$ (red), and **6**·THF (blue) and the corresponding ground species (dashed lines) together with **6** in a THF solution (green).

one hand, the low-energy bands of crystalline species **6**·THF are obviously red-shifted compared with those of crystalline species **6**·CH_2Cl_2 and **6**·$^1/_2CH_2ClCH_2Cl$. On the other hand, when the sample are thoroughly mechanically ground, the corresponding low-energy band is significantly red-shifted for **6**·CH_2Cl_2 and **6**·$^1/_2CH_2ClCH_2Cl$ whereas it is distinctly blue-shifted for **6**·THF (Figure 2). The XRD measurement revealed that the XRD patterns vanished entirely for all of the ground samples, indicating that the regular crystalline state was totally destroyed by mechanical grinding.[7c,d]

Upon excitation at wavelengths longer than 320 nm, crystalline species, including desolvated **6**, **6**·$^1/_2CH_2ClCH_2Cl$, and **6**·CH_2Cl_2, exhibit bright yellow luminescence with two vibronic-structured emission bands centered at 561 and 608 nm (Table 2). Crystalline species **6**·THF, however, displays bright red luminescence with an unstructured and broad emission band centered at 698 nm.

Luminescence Vapochromic Properties. Scheme 2 depicts the conversion processes of complex **6** in various forms of solid states in response to vapor, heat, and mechanical grinding. The vapo-, thermo-, and mechano-triggered emission spectral changes of complex **6** are presented in Figure 3. Photographic images of **6** in PMMA films are shown in Figure 4, showing remarkable luminescence color switches under UV light (365 nm) irradiation in response to vapor or mechanical stimuli.

When solid **6** is exposed to vapors of VOCs, including methanol, ethanol, furan, 2-methyltetrahydrofuran, acetone, acetonitrile, diethyl ether, ethyl acetate, *n*-hexane, toluene, benzene, pyridine, various halohydrocarbons, etc., bright yellow or orange luminescence is always observed with vibronic-structured emission bands at 561 and 608 nm. Nevertheless, upon exposure of **6** to vapor of THF, dioxane, or THP, bright red luminescence is exhibited with a broad, unstructured emission band centered at 698 nm (THF), 689 nm (dioxane), or 715 nm (THP). As shown in Figure 5, complex **6** shows selective phosphorescence vapochromic properties in response to THF, dioxane, or THP vapor with a drastic vapochromic response shift. Figure 6 shows reversible emission spectral changes of solid **6** in response to THF or CH_2ClCH_2Cl vapor in the reverse process, showing gradual interconversion between two vibronic-structured emission bands (561 and 608 nm) and a broad unstructured emission (~698 nm). The reversibility and reproducibility of the conversion processes have been also confirmed by the variations of the XRD diagrams recorded in a reversible vapochromic **6**·$^1/_2CH_2ClCH_2Cl$ ⇆ **6**·THF cycle. Figure 7 shows dynamic variations of the XRD patterns in the **6**·$^1/_2CH_2ClCH_2Cl$ → **6**·THF process upon exposure of the **6**·$^1/_2CH_2ClCH_2Cl$ sample to a saturated THF vapor as well as the corresponding variations of the XRD patterns in the **6**·THF → **6**·$^1/_2CH_2ClCH_2Cl$ reverse process upon exposure of the **6**·THF sample to CH_2ClCH_2Cl vapor at ambient temperature. Consequently, the THF-responsive vapochromic luminescence switch is totally reversible as demonstrated upon exposure of the solid sample in THF vapor and another organic vapor alternately. The conversion processes could be repeated for several exposure cycles without detectable decomposition of the solid materials.

As revealed by X-ray crystallography, both **6**·CH_2Cl_2 and **6**·$^1/_2CH_2ClCH_2Cl$ exhibit an antiparallel packing pattern in stacking of planar platinum(II) complex molecules with the shortest intermolecular Pt···Pt distances being >4.0 Å, implying that it is impossible to form Pt–Pt contacts. For **6**·THF, an alternately staggered and antiparallel packing pattern gives short [3.255(8) Å] and long [4.646(10) Å] Pt···Pt distances, respectively, leading to the formation of a dimeric structure through intermolecular Pt–Pt interaction, thus resulting in a lower ^{3}MLCT/^{3}LLCT energy level and thus a significant red shift of the emission as demonstrated by DFT studies (vide infra).

In our previous studies, it has been demonstrated that complex $Pt(Me_3SiC{\equiv}CbpyC{\equiv}CSiMe_3)(C{\equiv}CC_6H_5)_2$ (**1**)[7b]

dx.doi.org/10.1021/ic202421d | Inorg. Chem. 2012, 51, 5569–5579

Scheme 2. Interconversion Processes for Solid Materials Based on Complex 6

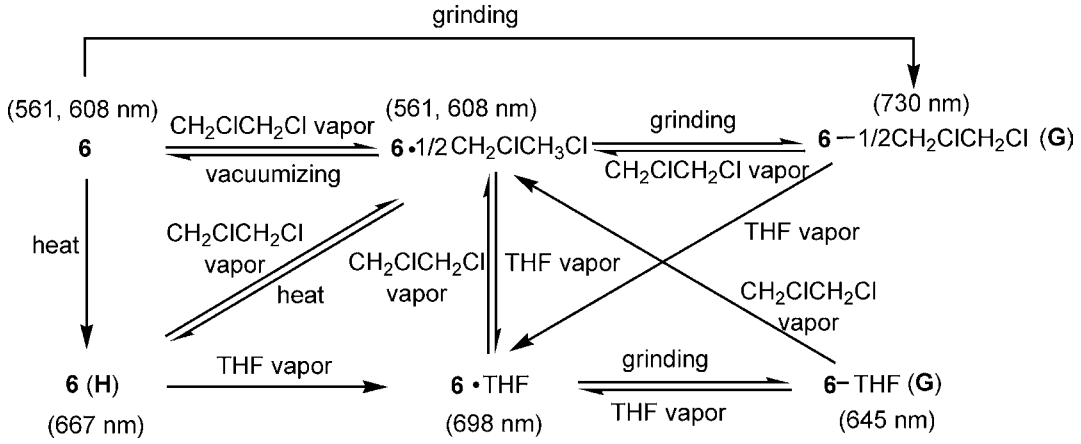

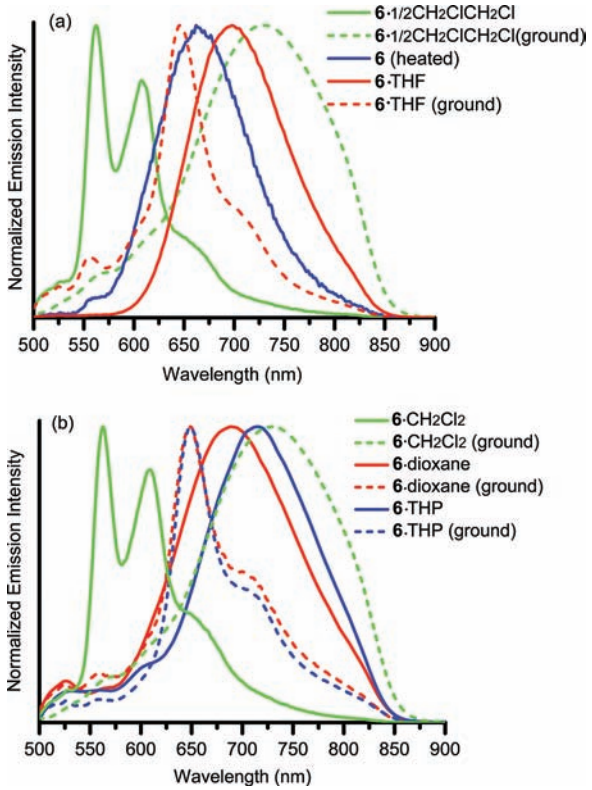

Figure 3. Solid-state emission spectra of crystalline and corresponding ground materials based on complex **6**·VOC at ambient temperature.

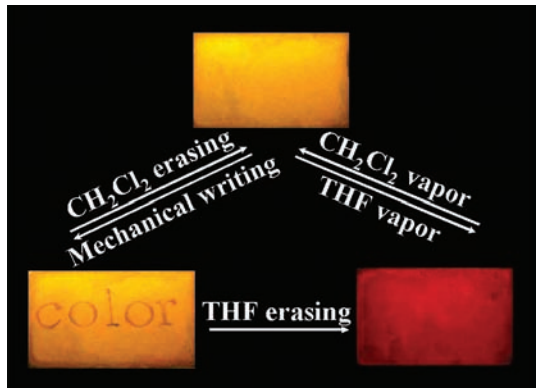

Figure 4. Photographic images of **6** in a PMMA film in response to CH_2Cl_2 vapor or mechanical stimuli under UV light (365 nm) irradiation.

is sensitive to CH_2Cl_2, $CHCl_3$, and CH_3I vapors with a significant vapochromic red shift of the emission from 562 and 603 nm to 762 nm. For bis(*σ*-fluorophenylacetylide) platinum-(II) complexes $Pt(Me_3SiC{\equiv}CbpyC{\equiv}CSiMe_3)(C{\equiv}CR)_2$ (R is C_6H_4F-2 for **2**, C_6H_4F-3 for **3**, and C_6H_4F-4 for **4**),[7c] **3** displays luminescence vapochromic behavior only to $CHCl_3$ vapor with a luminescence vapochromic red shift from 556 and 603 nm to 740 nm, whereas **4** is selectively sensitive to $CHCl_3$ and CH_2Cl_2 vapors with a luminescence vapochromic red shift from 562 and 608 nm to 765 nm ($CHCl_3$) or 760 nm (CH_2Cl_2). Complex $Pt(Me_3SiC{\equiv}CbpyC{\equiv}CSiMe_3)(C{\equiv}Cbpy)_2$ (**5**, C≡Cbpy=5-acetylide-2,2′-bipyridine)[7a] displays VOC-dependent luminescence vapochromic properties in response to several vapors, including acetone, *n*-hexane, ethyl acetate, $CHCl_3$, and THF, affording a progressively red-shifted vapochromic luminescence: 562(610sh) nm (acetone) → 617 nm (*n*-hexane) → 660 nm (ethyl acetate) → 729 nm ($CHCl_3$) → 747 nm (THF) depending on the shortest Pt···Pt distance induced by the inserted solvate molecules in the crystal lattices. It is demonstrated that the shorter the intermolecular Pt···Pt distances in **5**·VOC with various solvate VOCs, the more red-shifted the phosphorescence emission due to the lower energy levels of ^{3}MLCT/^{3}LLCT triplet states. These previous studies together with the results presented in this study suggest that the packing patterns in the stacking of planar platinum(II) moieties and consequently the shortest intermolecular Pt···Pt distances play a crucial role in determining the emission energy and the extent of the luminescence vapochromic response. Vapor-triggered luminescence switches are also affected by other types of intermolecular interactions, including short *π*−*π* contacts between pyridyl rings of functionalized 2,2′-bipyridine as well as host−guest interactions between planar platinum(II) moieties and solvate molecules through C−H···*π*(C≡C) and C−H···X (X = F, Cl, or Br) hydrogen bonds. It appears that the selectivity of luminescence vapochromism in $Pt(Me_3SiC{\equiv}CbpyC{\equiv}CSiMe_3)(C{\equiv}CR)_2$ (R is C_6H_5, C_6H_4F, or $C_6H_4CF_3$) is highly dependent on the R substituent of the acetylide ligands. When R is C_6H_5 (**1**)[7b] or C_6H_4F (**2**−**4**),[7c] phosphorescence emission in the corresponding platinum(II) complexes is usually sensitive to vapors of specific halohydrocarbons because of the formation of C−H···*π*(C≡C) and C−H···X (X=F, Cl) hydrogen bond interactions, thus stabilizing a staggered crystal packing to afford significant Pt−

dx.doi.org/10.1021/ic202421d | Inorg. Chem. 2012, 51, 5569−5579

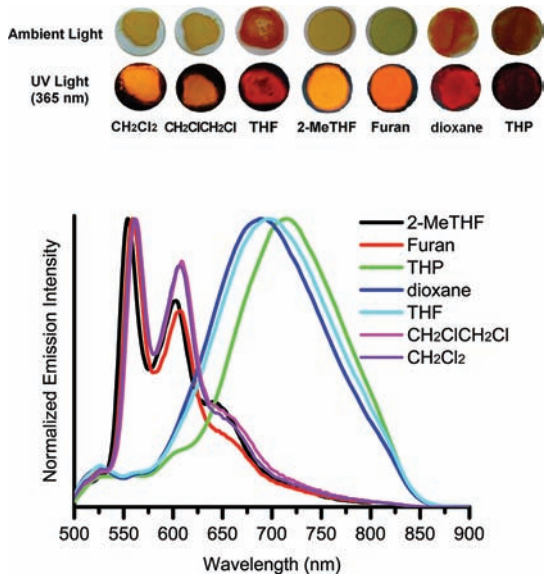

Figure 5. Photographic images (top) of **6** deposited on quartz slides upon exposure to selected organic vapors under ambient light and UV light irradiation (365 nm) and emission spectra (bottom) of **6** in the solid state upon exposure to various VOC vapors at ambient temperature, showing a broad unstructured emission centered at ~698 nm for THF, 689 nm for dioxane, and 715 nm for THP vapor, and two vibronic-structured bands at ~561 and ~608 nm for other VOC vapors.

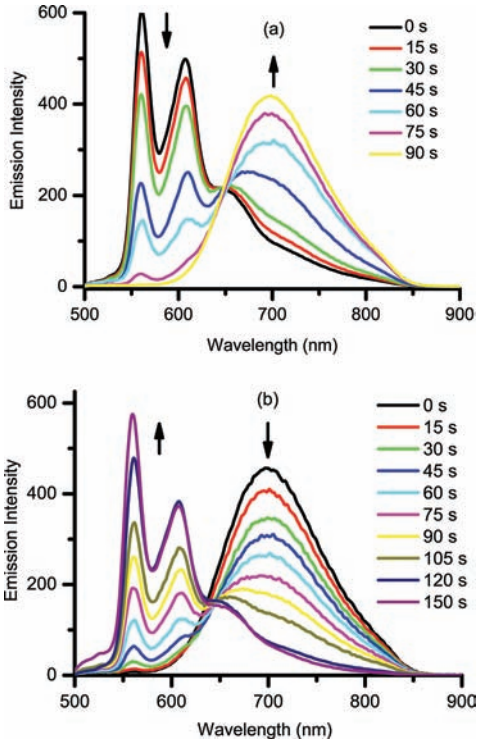

Figure 6. Emission spectral changes of solid **6**·$^1/_2CH_2ClCH_2Cl$ sample in response to THF vapor (top) and **6**·THF to CH_2ClCH_2Cl vapor (bottom), showing gradual interconversion between two vibronic-structured emission bands (561 and 608 nm) and a broad unstructured emission band (~698 nm).

Pt contact as a consequence of the solvate halohydrocarbon molecule being inserted into the crystal lattice. In contrast, when R is $C_6H_4CF_3$-4, the corresponding platinum(II) complex

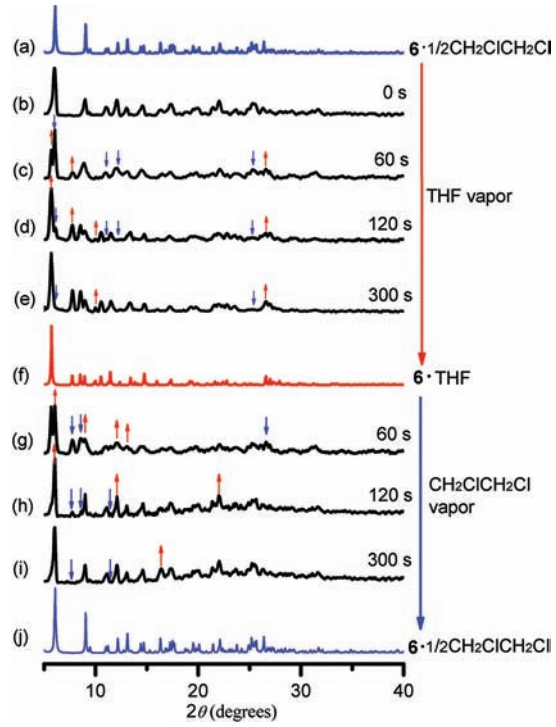

Figure 7. XRD diagrams recorded in a reversible vapochromic **6**·$^1/_2CH_2ClCH_2Cl$ ⇆ **6**·THF cycle, showing dynamic variations of the XRD patterns (c–e) in the **6**·$^1/_2CH_2ClCH_2Cl$ → **6**·THF process upon exposure of the **6**·$^1/_2CH_2ClCH_2Cl$ sample to a saturated THF vapor and those (g–i) in the **6**·THF → **6**·$^1/_2CH_2ClCH_2Cl$ reversed process upon exposure of the **6**·THF sample to CH_2ClCH_2Cl vapor at ambient temperature. (a and j) Simulated pattern of **6**·$^1/_2CH_2ClCH_2Cl$ from X-ray crystallography. (b) Measured pattern of **6**·$^1/_2CH_2ClCH_2Cl$. (f) Simulated pattern of **6**·THF from X-ray crystallography.

6 shows selective phosphorescence vapochromism in response to O-heterocyclic volatile compounds such as THF, dioxane, and THP with the emission at 561 and 608 nm being red-shifted to 698 nm (THF), 689 nm (dioxane), and 715 nm (THP), respectively. X-ray crystallography reveals that the staggered crystal packing with a short Pt···Pt distance [3.255(8) Å] in **6**·THF is highly stabilized by host–guest interactions between the platinum(II) moiety and solvate THF through C–H···O(THF) and F···H–C(THF) hydrogen bonds that are probably the force driving complex **6** to display selective luminescence vapochromism toward THF, dioxane, and THP.

Luminescence Mechanochromic Properties. When crystalline materials, including desolvated **6**, **6**·CH_2Cl_2, and **6**·$^1/_2CH_2ClCH_2Cl$, are ground in an agate mortar or crushed gently on a paper with a spatula, dramatic changes in color and luminescence with a drastic red shift of the emission are observed. When these solid samples are thoroughly ground, bright yellow luminescence with two vibronic-structured emission bands centered at 561 and 608 nm (Figure 3) converts immediately to weak red luminescence with a broad and unstructured band centered at 730 nm, affording a drastic mechanochromic red shift response. In contrast, when vapochromic crystalline species **6**·THF, **6**·dioxane, or **6**·THP is mechanically ground, bright red luminescence centered at 698 nm (THF), 689 nm (dioxane), or 715 nm (THP), respectively, is obviously blue-shifted to 645 nm with a more intense red emission, giving a remarkable mechanochromic blue

dx.doi.org/10.1021/ic202421d | Inorg. Chem. 2012, 51, 5569–5579

shift response. Both emission spectral and XRD studies suggest that the ground species from $6\cdot{}^1/_2CH_2ClCH_2Cl$ (Figure S14 of the Supporting Information and Figure 8) or **6**·THF (Figure S15 of the Supporting Information and Figure 8) could perfectly revert to the original crystalline state upon being exposed to the corresponding vapors. Upon exposure of the ground samples to CH_2ClCH_2Cl or THF vapor, the broad, unstructured emission band centered at 730 or 645 nm could progressively revert to two vibronic-structured bands at 561 and 608 nm in response to CH_2ClCH_2Cl vapor (Figure S15 of the Supporting Information) or restored to an unstructured band centered at 698 nm in response to THF vapor (Figure S16 of the Supporting Information). The XRD studies indicate that the diffraction patterns of **6**·VOC disappear entirely when they are thoroughly ground[7c,d] but could be restored perfectly to the original XRD patterns upon sufficient exposure to the corresponding VOC vapors. Figure 8 depicts the XRD diagrams in a mechanochromic cycle for $6\cdot{}^1/_2CH_2ClCH_2Cl$ and **6**·THF, showing the XRD patterns for the crystalline and the ground species together with the changes in XRD patterns during the restoring process from the ground sample in response to CH_2ClCH_2Cl or THF vapor.

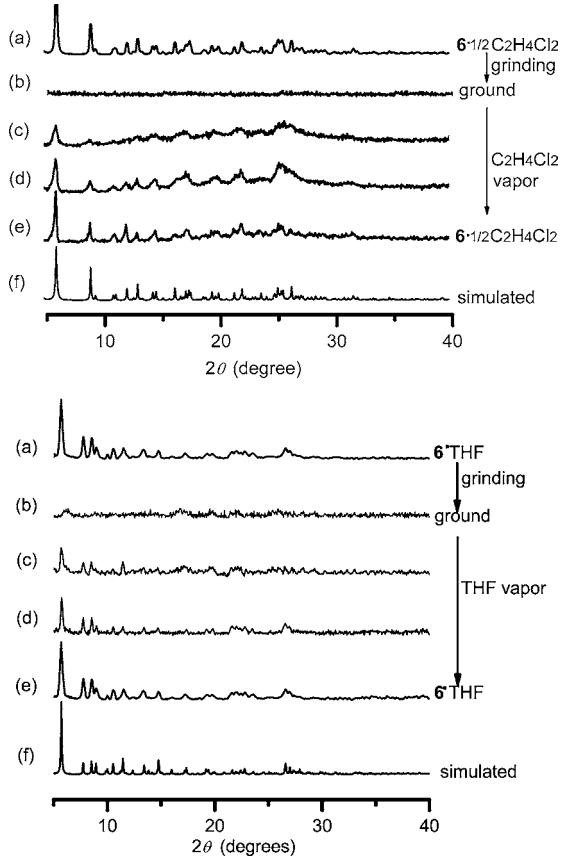

Figure 8. XRD diagrams in a mechanochromic cycle for $6\cdot{}^1/_2CH_2ClCH_2Cl$ (top) and **6**·THF (bottom), showing the measured (a) and simulated (f) patterns for the unground sample, the measured pattern for the ground sample (b), and dynamic variations (c–e) of the XRD patterns for the ground samples in response to CH_2ClCH_2Cl (top) or THF (bottom) vapor in the reversed process.

Thermogravimetric studies (Figures S4–S6 of the Supporting Information) show that when **6**·VOC (VOC = THF, CH_2Cl_2, or CH_2ClCH_2Cl) is thoroughly ground, solvate VOC molecules are totally lost with crystalline states converted to amorphous phases. Nevertheless, the loss of solvate is not a prerequisite of luminescence mechanochromism for **6**·VOC because desolvated crystalline species **6** exhibits the same mechanoluminescence as $6\cdot{}^1/_2CH_2ClCH_2Cl$. Noticeably, regular crystal arrangements for both crystalline species $6\cdot{}^1/_2CH_2ClCH_2Cl$ and **6**·THF are totally damaged upon the samples being thoroughly ground to afford amorphous species, but they belong to two different amorphous states. The ground amorphous species from $6\cdot{}^1/_2CH_2ClCH_2Cl$ displays weak red luminescence centered at 730 nm, whereas the ground species from **6**·THF is strongly emissive at 645 nm. However, it appears that heating of both ground species with different amorphous morphs could result in the same new crystalline state as suggested by XRD measurements (Figure S21 of the Supporting Information).

Our previous studies have shown that when the crystalline materials $Pt(Me_3SiC{\equiv}CbpyC{\equiv}CSiMe_3)(C{\equiv}CR)_2$ (R is C_6H_4F-2 for **2**, C_6H_4F-3 for **3**, and C_6H_4F-4 for **4**)[7c] and $Pt(Me_3SiC{\equiv}Cbpy)(C{\equiv}CR)_2$ [R is C_6H_5 for **7**or $C_6H_4Bu^t$-4 for **8**; $Me_3SiC{\equiv}Cbpy$ = 5-(trimethylsilylethynyl)-2,2′-bipyridine][7d] are mechanically ground or crushed, a drastic emission red shift is always observed with bright yellow or yellow-green luminescence converted to dark red. Upon being mechanically ground, planar platinum(II) molecules are likely packed in proximity through Pt–Pt interaction to form a dimeric or an aggregate structure, resulting in a conversion from a ^{3}MLCT/^{3}LLCT emissive state in the crystalline state to a ^{3}MMLCT triplet state in the amorphous phase and thus a significant red shift of the emission. By comparison, solvate-dependent mechanoluminescence properties in crystalline materials **6**·VOC are observed for the first time. While crystalline materials such as desolvated **6**, $6\cdot CH_2Cl_2$, and $6\cdot{}^1/_2CH_2ClCH_2Cl$ exhibit a grinding-triggered emission red shift from vibronic-structured bands at 561 and 608 nm to unstructured broad emission centered at 730 nm, the emission at 698 nm (THF), 689 nm (dioxane), or 715 nm (THP) is distinctly blue-shifted to 645 nm when vapochromic crystalline materials **6**·THF, **6**·dioxane, and **6**·THP are mechanically ground. Consequently, this study indicates that mechanical grinding could lead to a luminescence red shift as well as a blue shift depending on the solvate molecules, in which mechanical force not only induces planar platinum(II) molecules to be packed in the proximity through Pt–Pt or π–π interaction in most cases but also could disrupt ordered close packing in stacking of planar platinum(II) moieties.

Thermo-Triggered Luminescence Changes. When desolvated **6**, $6\cdot{}^1/_2CH_2ClCH_2Cl$, or $6\cdot CH_2Cl_2$ is heated at 120 °C, bright yellow luminescence with two vibronic-structured emission bands at 561 and 608 nm turns into red luminescence with a broad structureless emission band centered at 667 nm (Figure 3), suggesting the occurrence of thermo-triggered luminescence change with the loss of solvate CH_2ClCH_2Cl or CH_2Cl_2. Upon exposure of the heated sample to CH_2ClCH_2Cl or CH_2Cl_2 vapor, the unstructured emission band centered at 667 nm could reversibly revert to two vibronic-structured emission bands at 561 and 608 nm in the original species $6\cdot{}^1/_2CH_2ClCH_2Cl$ or $6\cdot CH_2Cl_2$. Temperature-dependent XRD measurement (Figure S20 of the Supporting Information) on desolvated **6** in the temperature range of 25–145 °C demonstrates that a crystalline-state transition occurs indeed at ~85 °C, as revealed by the distinct variations in XRD patterns. Heating of **6**·THF at 120 °C, however, could not

dx.doi.org/10.1021/ic202421d | Inorg. Chem. 2012, 51, 5569–5579

induce conversion of the emission centered at 698 nm into emission at 667 nm, in which the luminescence at 698 nm is instead quenched upon heating. This implies that the loss of solvate THF gives another desolvated morph, which is different from that produced by the loss of solvate CH_2ClCH_2Cl or CH_2Cl_2 in $\mathbf{6}\cdot{}^1/_2CH_2ClCH_2Cl$ or $\mathbf{6}\cdot CH_2Cl_2$. The XRD measurements (Figure S19 of the Supporting Information) reveal unambiguously that upon being heated at 120 °C, the species formed by the loss of solvate THF differs distinctly from that produced by loss of solvate CH_2ClCH_2Cl or CH_2Cl_2 in $\mathbf{6}\cdot{}^1/_2CH_2ClCH_2Cl$ or $\mathbf{6}\cdot CH_2Cl_2$. Thus, our experiments suggest that desolvated **6** exhibits polymorphism that differs in their solid-state packing arrangements, including at least three crystalline and two noncrystalline morphs as demonstrated by their differences in XRD patterns (Figure S19 of the Supporting Information). Three crystalline phases are caused by desolvation of $\mathbf{6}\cdot{}^1/_2CH_2ClCH_2Cl$ or $\mathbf{6}\cdot CH_2Cl_2$ in vacuum at ambient temperature with emission at 561 and 608 nm, desolvation by heating $\mathbf{6}\cdot{}^1/_2CH_2ClCH_2Cl$ or $\mathbf{6}\cdot CH_2Cl_2$ at temperatures higher than 85 °C with emission at 667 nm, and desolvation by heating **6**·THF at 120 °C with the emission quenched. Two noncrystalline phases originate from desolvation by mechanical grinding on crystalline species $\mathbf{6}\cdot{}^1/_2CH_2ClCH_2Cl$ and **6**·THF with emission occurring at 730 and 645 nm, respectively. Nevertheless, heating of the ground species with different amorphous morphs results in the same new crystalline state according to the XRD measurements (Figure S21 of the Supporting Information), in which the emission is always quenched when the ground species are further heated.

DFT Computational Studies. Time-dependent DFT (TD-DFT) calculations at the PBE1PBE level were conducted to elucidate the frontier orbital components and spectral transition characteristics of **6** in a CH_2Cl_2 solution using the ground-state structure (Table S1 of the Supporting Information) optimized by the DFT method. Partial molecular orbital compositions (percentage) in the ground state and transition properties of **6** are provided as Supporting Information (Tables S2 and S3). On the basis of the TD-DFT studies, the intense UV absorptions below 370 nm are featured with an intraligand (IL) $\pi \rightarrow \pi^*$ transition ($Me_3SiC{\equiv}CbpyC{\equiv}CSiMe_3$), mixed with some ^{1}LLCT/^{1}MLCT character. The low-energy of HOMO → LUMO, HOMO-1 → LUMO, and HOMO-2 → LUMO absorption transitions arise primarily from $\pi(C{\equiv}CC_6H_4CF_3\text{-}4) \rightarrow \pi^*(Me_3SiC{\equiv}CbpyC{\equiv}CSiMe_3)$ ^{1}LLCT and $5d(Pt) \rightarrow \pi^*(Me_3SiC{\equiv}CbpyC{\equiv}CSiMe_3)$ ^{1}MLCT states. Likewise, the triplet-state emission, which is primarily characteristic of HOMO → LUMO and HOMO-3 → LUMO transitions, can be ascribed to ^{3}LLCT/^{3}MLCT triplet excited states together with some ^{3}IL character of $Me_3SiC{\equiv}CbpyC{\equiv}CSiMe_3$. Such a significant contribution from the ^{3}IL state of $Me_3SiC{\equiv}CbpyC{\equiv}CSiMe_3$ in complex **6** leads to distinctly vibronic-structured emission at 568 (608sh) nm in a fluid CH_2Cl_2 solution, which is strikingly different from the structureless solution emission bands found in analogues $Pt(Me_3SiC{\equiv}CbpyC{\equiv}CSiMe_3)(C{\equiv}CR)_2$ (R is C_6H_5 for **1**, C_6H_4F-2 for **2**, C_6H_4F-3 for **3**, C_6H_4F-4 for **4**, and bpy for **5**).[7] The distinctly blue-shifted emission of **6** (568 and 608sh nm) compared with that of **1** (616 nm)[7b] in a fluid CH_2Cl_2 solution is well elucidated by a larger HOMO−LUMO gap of **6** (3.12 eV) compared to that of **1** (2.904 eV)[7b] because of the introduction of an electron-withdrawing CF_3 group into phenylacetylide in **6**. Both the calculated singlet and triplet excitation transitions (Table S3 of the Supporting Information) coincide well with the measured UV−vis electronic absorption (Figure S24 of the Supporting Information) and emission spectral data.

To interpret the UV−vis and emission spectral differences in crystalline species **6**·VOC with different solvate VOCs and explore the origin of THF-triggered luminescence vapochromism, TD-DFT studies were performed on crystalline morphs $\mathbf{6}\cdot{}^1/_2CH_2ClCH_2Cl$ and **6**·THF using a pair of square-planar platinum(II) moieties having the shortest intermolecular Pt···Pt distance. The relevant calculation data, including molecular orbital compositions (percentages) and transition properties, are provided as Supporting Information (Tables S4−S7). To gain intuitive insight into the changes in the frontier orbitals resulting from the inserted solvate VOC in crystal lattices, Figure 9 depicts the energy level of frontier molecular orbitals

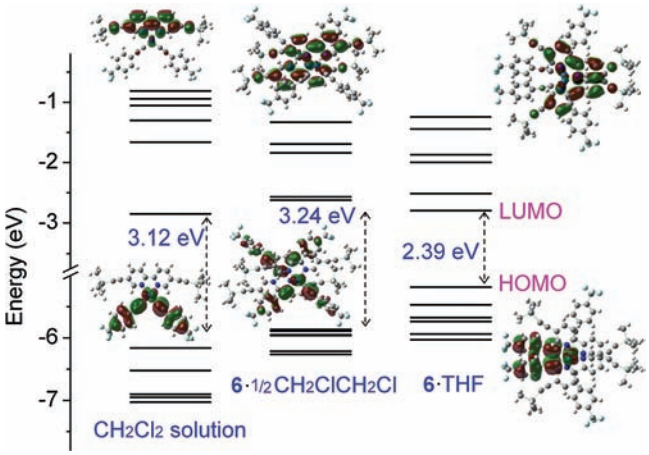

Figure 9. Plots of the energy level of frontier molecular orbitals HOMO-5 to LUMO+5 for **6** in a CH_2Cl_2 solution, solid-state $\mathbf{6}\cdot{}^1/_2CH_2ClCH_2Cl$, and **6**·THF in the ground states by the TD-DFT method at the PBE1PBE level, together with the electron density diagrams of the HOMO and LUMO orbitals.

HOMO-5 to LUMO+5 for **6** in a CH_2Cl_2 solution, solid-state $\mathbf{6}\cdot{}^1/_2CH_2ClCH_2Cl$, and **6**·THF together with the electron density diagrams of the HOMO and LUMO.

Analogous to those in a CH_2Cl_2 solution, the corresponding low-energy absorption and emission in solid-state $\mathbf{6}\cdot{}^1/_2CH_2ClCH_2Cl$ (Tables S4 and S5 of the Supporting Information) and **6**·THF (Tables S6 and S7 of the Supporting Information) originate primarily from LLCT/MLCT excited states, comparable to those found in analogues $Pt(Me_3SiC{\equiv}CbpyC{\equiv}CSiMe_3)(C{\equiv}CR)_2$ (R is C_6H_5 for **1**, C_6H_4F-2 for **2**, C_6H_4F-3 for **3**, C_6H_4F-4 for **4**, and bpy for **5**).[7] Compared with that in $\mathbf{6}\cdot{}^1/_2CH_2ClCH_2Cl$ (Figure 9), the HOMO level is significantly higher whereas the LUMO level is slightly lowered in **6**·THF, thus resulting in a much smaller HOMO−LUMO energy gap in **6**·THF (2.39 eV) than in $\mathbf{6}\cdot{}^1/_2CH_2ClCH_2Cl$ (3.24 eV). Via careful examination of the HOMO compositions (Tables S4 and S6 of the Supporting Information), we found that the contribution of the d_{z^2} (Pt) orbital to the HOMO in **6**·THF (7.42%) is much larger than that in $\mathbf{6}\cdot{}^1/_2CH_2ClCH_2Cl$ (0.21%). When the intermolecular Pt···Pt distance is sufficiently short (<3.5 Å) to form Pt−Pt contacts, it has been demonstrated that the HOMO is featured with the $d\sigma^*$ nature resulting from σ-overlap between two d_{z^2} (Pt) orbitals with a higher energy level in the aggregate species than that of individual the d_{z^2} (Pt) orbital in the monomeric moiety, thus

dx.doi.org/10.1021/ic202421d | Inorg. Chem. 2012, 51, 5569−5579

inducing a smaller HOMO−LUMO energy gap that is significantly perturbed by the Pt···Pt distances.[54] As demonstrated by X-ray crystallography, the antiparallel oriented planar platinum(II) moieties in **6**·$^1/_2CH_2ClCH_2Cl$ [4.262(11) Å] afford a Pt···Pt distance much longer than that in **6**·THF [3.255(8) Å] with two neighboring platinum(II) molecules arranged in a staggered pattern. Consequently, the DFT studies of **6**·THF and **6**·$^1/_2CH_2ClCH_2Cl$ reveal unambiguously that THF-triggered absorption and emission red shifts arise most likely from remarkably enhanced intermolecular Pt−Pt interaction upon insertion of solvate THF into the crystal lattices to induce a staggered pattern of packing of square-planar platinum(II) moieties. Furthermore, the results of this DFT study agree well with the data for previously described complexes $Pt(Me_3SiC{\equiv}CbpyC{\equiv}CSiMe_3)(C{\equiv}CR)_2$ (R is C_6H_5 for **1**, C_6H_4F-2 for **2**, C_6H_4F-3 for **3**, and C_6H_4F-4 for **4**),[7] in which vapochromic crystalline materials **1**·$CHCl_3$, **3**·$CHCl_3$, **4**·CH_2Cl_2, and **4**·$CHCl_3$ always originate from an increased contribution from intermolecular Pt−Pt interaction upon insertion of solvate $CHCl_3$ or CH_2Cl_2 molecules into crystal lattices; thus, the ^{3}MLCT/^{3}LLCT emissive state is converted to a lower energy level.

CONCLUSIONS

Vapo-, thermo-, and mechano-responsive phosphorescence switches of a bis(σ-acetylide) platinum(II) complex with 5,5′-bis(trimethylsilylethynyl)-2,2′-bipyridine and 4-(trifluoromethylphenyl)acetylide are described. Depending on solid forms and structures, the materials based on this platinum(II) complex show yellow to red luminescence with five different emission wavelengths. In response to vapors of volatile O-heterocyclic compounds such as THF, dioxane, and THP, bright yellow luminescence of the materials at 561 and 608 nm converts to red luminescence centered at 698 nm (THF), 689 nm (dioxane), and 715 nm (THP), respectively, with significant vapochromic response shifts. When crystalline **6**·VOC samples are mechanically ground, the emission is obviously blue-shifted for **6**·THF, **6**·dioxane, or **6**·THP and drastically red-shifted for **6**, **6**·CH_2Cl_2, or **6**·$^1/_2CH_2ClCH_2Cl$. Upon being heated to >85 °C, crystalline species **6**·VOC, except when the VOC was THF, dioxane, or THP, turns into another crystalline phase with emission at 561 and 608 nm red-shifted to 667 nm. The vapo-, thermo-, and mechano-triggered luminescence changes are mostly reversible with the conversion from one state to another by vapor adsorption or recrystallization. The multistimulus-responsive luminescence and color switches are most likely relevant to the variations in intermolecular interactions in packing of planar platinum(II) moieties, which are significantly perturbed by solvate molecules, mechanical force, or heating (Table 1).

ASSOCIATED CONTENT

Supporting Information

Figures giving additional UV−vis and emission spectra, diagrams of XRD patterns, tables and figures giving DFT calculation data, and an X-ray crystallographic file in CIF format for the determination of the structures of compounds **6**·$^1/_2CH_2ClCH_2Cl$, **6**·CH_2Cl_2, and **6**·THF. This material is available free of charge via the Internet at http://pubs.acs.org.

AUTHOR INFORMATION

Corresponding Author

*E-mail: czn@fjirsm.ac.cn.

Notes

The authors declare no competing financial interest.

ACKNOWLEDGMENTS

We are grateful for financial support from the NSFC (20931006, U0934003, and 91122006), the 973 project (2007CB815304) from MSTC, and the NSF of Fujian Province (2011J01065).

REFERENCES

(1) (a) Chan, C. W.; Cheng, L. K.; Che, C. M. *Coord. Chem. Rev.* **1994**, *132*, 87. (b) Hissler, M.; McGarrah, J. E.; Connick, W. B.; Geiger, D. K.; Cummings, S. D.; Eisenberg, R. *Coord. Chem. Rev.* **2000**, *208*, 115. (c) Castellano, F. N.; Pomestchenko, I. E.; Shikhova, E.; Hua, F.; Muro, M. L.; Rajapakse, N. *Coord. Chem. Rev.* **2006**, *250*, 1819. (d) Gareth Williams, J. A. *Top. Curr. Chem.* **2007**, *281*, 205.

(2) Hissler, M.; Connick, W. B.; Geiger, D. K.; McGarrah, J. E.; Lipa, D.; Lachicotte, R. J.; Eisenberg, R. *Inorg. Chem.* **2000**, *39*, 447.

(3) Chan, S.-C.; Chan, M. C. W.; Wang, Y.; Che, C.-M.; Cheung, K.-K.; Zhu, N. *Chem.—Eur. J.* **2001**, *7*, 4180.

(4) Pomestchenko, I. E.; Luman, C. R.; Hissler, M.; Ziessel, R.; Castellano, F. N. *Inorg. Chem.* **2003**, *42*, 1394.

(5) Whittle, C. E.; Weinstein, J. A.; George, M. W.; Schanze, K. S. *Inorg. Chem.* **2001**, *40*, 4053.

(6) (a) Lu, W.; Chan, M. C. W.; Zhu, N.; Che, C.-M.; He, Z.; Wong, K.-Y. *Chem.—Eur. J.* **2003**, *9*, 6155. (b) Kui, S. C. F.; Chui, S. S.-Y.; Che, C.-M.; Zhu, N. *J. Am. Chem. Soc.* **2006**, *128*, 8297.

(7) (a) Ni, J.; Zhang, L.-Y.; Wen, H.-M.; Chen, Z.-N. *Chem. Commun.* **2009**, 3801. (b) Ni, J.; Wu, Y.-H.; Zhang, L.-Y.; Chen, Z.-N. *Inorg. Chem.* **2009**, *48*, 10202. (c) Ni, J.; Zhang, X.; Wu, Y.-H.; Zhang, L.-Y.; Chen, Z.-N. *Chem.—Eur. J.* **2011**, *17*, 1171. (d) Ni, J.; Zhang, X.; Qiu, N.; Wu, Y.-H.; Zhang, L.-Y.; Zhang, J.; Chen, Z.-N. *Inorg. Chem.* **2011**, *50*, 9090.

(8) (a) Hudson, Z. M.; Sun, C.; Harris, K. J.; Lucier, B. E. G.; Schurko, R. W.; Wang, S. *Inorg. Chem.* **2011**, *50*, 3447. (b) Pang, J.; Marcotte, E. J.-P.; Seward, C.; Brown, R. S.; Wang, S. *Angew. Chem., Int. Ed.* **2001**, *40*, 4042.

(9) (a) Du, P.; Schneider, J.; Brennessel, W. W.; Eisenberg, R. *Inorg. Chem.* **2008**, *47*, 69. (b) Wadas, T. J.; Wang, Q.-M.; Kim, Y.-j.; Flaschenreim, C.; Blanton, T. N.; Eisenberg, R. *J. Am. Chem. Soc.* **2004**, *126*, 16841. (c) Du, P. *Inorg. Chim. Acta* **2010**, *363*, 1355.

(10) (a) Buss, C. E.; Mann, K. R. *J. Am. Chem. Soc.* **2002**, *124*, 1031. (b) Drew, S. M.; Smith, L. I.; McGee, K. A.; Mann, K. R. *Chem. Mater.* **2009**, *21*, 3117. (c) McGee, K. A.; Marquardt, B. J.; Mann, K. R. *Inorg. Chem.* **2008**, *47*, 9143. (d) Dylla, A. G.; Janzen, D. E.; Pomije, M. K.; Mann, K. R. *Organometallics* **2007**, *26*, 6243.

(11) (a) Grove, L. J.; Rennekamp, J. M.; Jude, H.; Connick, W. B. *J. Am. Chem. Soc.* **2004**, *126*, 1594. (b) Grove, L. J.; Oliver, A. G.; Krause, J. A.; Connick, W. B. *Inorg. Chem.* **2008**, *47*, 1408.

(12) Muro, M. L.; Daws, C. A.; Castellano, F. N. *Chem. Commun.* **2008**, 6134.

(13) (a) Kato, M.; Omura, A.; Toshikawa, A.; Kishi, S.; Sugimoto, Y. *Angew. Chem., Int. Ed.* **2002**, *41*, 3183. (b) Kato, M. *Bull. Chem. Soc. Jpn.* **2007**, *80*, 287. (c) Kobayashi, A.; Yonemura, T.; Kato, M. *Eur. J. Inorg. Chem.* **2010**, 2465.

(14) Lee, C.-S.; Zhuang, R. R.; Sabiah, S.; Wang, J.-C.; Hwang, W.-S.; Lin, I. J. B. *Organometallics* **2011**, *30*, 3897.

(15) Pattacini, R.; Giansante, C.; Ceroni, P.; Maestri, M.; Braunstein, P. *Chem.—Eur. J.* **2007**, *13*, 10117.

(16) Fornies, J.; Fuertes, S.; Lopez, J. A.; Martin, A.; Sicilia, V. *Inorg. Chem.* **2008**, *47*, 7166.

(17) Rivera, E. J.; Barbosa, C.; Torres, R.; Grove, L.; Taylor, S.; Connick, W. B.; Clearfieldc, A.; Colon, J. L. *J. Mater. Chem.* **2011**, *21*, 15899.

(18) (a) Mathew, I.; Sun, W. *Dalton Trans.* **2010**, *39*, 5885. (b) Choi, S. J.; Kuwabara, J.; Nishimura, Y.; Arai, T.; Kanbara, T. *Chem. Lett.* **2012**, *41*, 65–67.
(19) Li, Y.-J.; Deng, Z.-Y.; Xu, X.-F.; Wu, H.-B.; Cao, Z.-X.; Wang, Q.-M. *Chem. Commun.* **2011**, *47*, 9179.
(20) Cariati, E.; Bu, X.; Ford, P. C. *Chem. Mater.* **2000**, *12*, 3385.
(21) Strasser, C. E.; Catalano, V. J. *J. Am. Chem. Soc.* **2010**, *132*, 10009.
(22) (a) Laguna, A.; Lasanta, T.; Lopez-de-Luzuriaga, J. M.; Monge, M.; Naumov, P.; Olmos, M. E. *J. Am. Chem. Soc.* **2010**, *132*, 456. (b) Lasanta, T.; Olmos, M. E.; Laguna, A.; Lopez-de-Luzuriaga, J. M.; Naumov, P. *J. Am. Chem. Soc.* **2011**, *133*, 16358. (c) Fernandez, E. J.; Lopez-de-Luzuriaga, J. M.; Monge, M.; Olmos, M. E.; Puelles, R. C.; Laguna, A.; Mohamed, A. A.; Fackler, J. P., Jr. *Inorg. Chem.* **2008**, *47*, 8069. (d) Fernandez, E. J.; Lopez-de-Luzuriaga, J. M.; Monge, M.; Montiel, M.; Olmos, M. E.; Perez, J.; Laguna, A.; Mendizabai, F.; Mohamed, A. A.; Fackler, J. P., Jr. *Inorg. Chem.* **2004**, *43*, 3573.
(23) Osawa, M.; Kawata, I.; Igawa, S.; Hoshino, M.; Fukunaga, T.; Hashizume, D. *Chem.—Eur. J.* **2010**, *16*, 12114.
(24) (a) Lim, S. H.; Olmstead, M. M.; Balch, A. L. *J. Am. Chem. Soc.* **2011**, *133*, 10229. (b) White-Morris, R. L.; Olmstead, M. M.; Attar, S.; Balch, A. L. *Inorg. Chem.* **2005**, *44*, 5021.
(25) Rawashdeh-Omary, M. A.; Rashdan, M. D.; Dharanipathi, S.; Elbjeirami, O.; Rameshb, P.; Rasika Dias, H. V. *Chem. Commun.* **2011**, *47*, 1160.
(26) Liu, Z.; Bian, Z.; Bian, J.; Li, Z.; Nie, D.; Huang, C. *Inorg. Chem.* **2008**, *47*, 8025.
(27) (a) Abe, T.; Suzuki, T.; Shinozaki, K. *Inorg. Chem.* **2010**, *49*, 1794. (b) Mizukami, S.; Houjou, H.; Sugaya, K.; Koyama, E.; Tokuhisa, H.; Sasaki, T.; Kanesato, M. *Chem. Mater.* **2005**, *17*, 50.
(28) Balch, A. L. *Angew. Chem., Int. Ed.* **2009**, *48*, 2641.
(29) (a) Lee, Y.-A.; Eisenberg, R. *J. Am. Chem. Soc.* **2003**, *125*, 7778. (b) Schneider, J.; Lee, Y.-A.; Perez, J.; Brennessel, W. W.; Flaschenriem, C.; Eisenberg, R. *Inorg. Chem.* **2008**, *47*, 957.
(30) (a) Assefa, Z.; Omary, M. A.; McBurnett, B. G.; Mohamed, A. A.; Patterson, H. H.; Staples, R. J.; Fackler, J. P. *Inorg. Chem.* **2002**, *41*, 6274. (b) Catalano, V. J.; Horner, S. J. *Inorg. Chem.* **2003**, *42*, 8430.
(31) (a) Kuchison, A. M.; Wolf, M. O.; Patrick, B. O. *Chem. Commun.* **2009**, 7387. (b) Ito, H.; Saito, T.; Oshima, N.; Kitamura, N.; Ishizaka, S.; Hinatsu, Y.; Wakeshima, M.; Kato, M.; Tsuge, K.; Sawamura, M. *J. Am. Chem. Soc.* **2008**, *130*, 10044.
(32) Perruchas, S.; Le Goff, X. F.; Maron, S.; Maurin, I.; Guillen, F.; Garcia, A.; Gacoin, T.; Boilot, J.-P. *J. Am. Chem. Soc.* **2010**, *132*, 10967–10969.
(33) Bi, H.; Chen, D.; Li, D.; Yuan, Y.; Xia, D.; Zhang, Z.; Zhang, H.; Wang, Y. *Chem. Commun.* **2011**, *47*, 4135.
(34) Tsukuda, T.; Kawase, M.; Dairiki, A.; Matsumoto, K.; Tsubomura, T. *Chem. Commun.* **2010**, *46*, 1905.
(35) Abe, T.; Itakura, T.; Ikeda, N.; Shinozaki, K. *Dalton Trans.* **2009**, 711.
(36) Tzeng, B.-C.; Chang, T.-Y.; Sheu, H.-S. *Chem.—Eur. J.* **2010**, *16*, 9990.
(37) Liao, C.-T.; Chen, H.-H.; Hsu, H.-F.; Poloek, A.; Yeh, H.; Chi, Y.; Wang, K.-W.; Lai, C.-H.; Lee, G.-H.; Shih, C.-W.; Chou, P.-T. *Chem.—Eur. J.* **2011**, *17*, 546.
(38) Chan, K. H.-Y.; Chow, H.-S.; Wong, K. M.-C.; Yeung, M. C.-L.; Yam, V. W.-W. *Chem. Sci.* **2010**, *1*, 477.
(39) Fornies, J.; Sicilia, V.; Casas, J. M.; Martin, A.; Lopez, J. A.; Larraz, C.; Borja, P.; Ovejero, C. *Dalton Trans.* **2011**, *40*, 2898.
(40) Perruchas, S.; Tard, C.; Le Goff, X. F.; Fargues, A.; Garcia, A.; Kahlal, S.; Saillard, J.-Y.; Gacoin, T.; Boilot, J.-P. *Inorg. Chem.* **2011**, *50*, 10682.
(41) Rachford, A. A.; Castellano, F. N. *Inorg. Chem.* **2009**, *48*, 10865.
(42) Kato, M.; Kosuge, C.; Morii, K.; Ahn, J. S.; Kitagawa, H.; Mitani, T.; Matsushita, M.; Kato, T.; Yano, S.; Kimura, M. *Inorg. Chem.* **1999**, *38*, 1638.
(43) Grosshenny, V.; Romero, F. M.; Ziessel, R. *J. Org. Chem.* **1997**, *62*, 1491.
(44) (a) Demas, J. N.; Crosby, G. A. *J. Phys. Chem.* **1971**, *75*, 991. (b) Chan, S. C.; Chan, M. C. W.; Wang, Y.; Che, C. M.; Cheung, K. K.; Zhu, N. *Chem.—Eur. J.* **2001**, *7*, 4180.
(45) Sheldrick, G. M. *SHELXL-97, Program for the Refinement of Crystal Structures*; University of Göttingen: Göttingen, Germany, 1997.
(46) Becke, A. D. *J. Chem. Phys.* **1993**, *98*, 5648.
(47) Casida, M. E.; Jamorski, C.; Casida, K. C.; Salahub, D. R. *J. Chem. Phys.* **1998**, *108*, 4439.
(48) Stratmann, R. E.; Scuseria, G. E.; Frisch, M. J. *J. Chem. Phys.* **1998**, *109*, 8218.
(49) Perdew, J. P.; Burke, K.; Ernzerhof, M. *Phys. Rev. Lett.* **1997**, *78*, 3865.
(50) (a) Cossi, M.; Scalmani, G.; Regar, N.; Barone, V. *J. Chem. Phys.* **2002**, *117*, 43. (b) Barone, V.; Cossi, M. *J. Chem. Phys.* **1997**, *107*, 3210.
(51) (a) Andrae, D.; Hauessermann, U.; Dolg, M.; Preuss, H. *Theor. Chim. Acta* **1990**, *77*, 123. (b) Schwerdtfeger, P.; Dolg, M.; Schwarz, W. H. E.; Bowmaker, G. A.; Boyd, P. D. W. *J. Chem. Phys.* **1989**, *91*, 1762. (c) Dolg, M.; Wedig, U.; Stoll, H.; Preuss, H. *J. Chem. Phys.* **1987**, *86*, 866.
(52) (a) Pyykkö, P.; Runeberg, N.; Mendizabal, F. *Chem.—Eur. J.* **1997**, *3*, 1451. (b) Pyykkö, P.; Mendizabal, F. *Chem.—Eur. J.* **1997**, *3*, 1458.
(53) Frisch, M. J.; Trucks, G. W.; Schlegel, H. B.; Scuseria, G. E.; Robb, M. A.; Cheeseman, J. R.; Montgomery, J. A., Jr.; Vreven, T.; Kudin, K. N.; Burant, J. C.; Millam, J. M.; Iyengar, S. S.; Tomasi, J.; Barone, V.; Mennucci, B.; Cossi, M.; Scalmani, G.; Rega, N.; Petersson, G. A.; Nakatsuji, H.; Hada, M.; Ehara, M.; Toyota, K.; Fukuda, R.; Hasegawa, J.; Ishida, M.; Nakajima, T.; Honda, Y.; Kitao, O.; Nakai, H.; Klene, M.; Li, X.; Knox, J. E.; Hratchian, H. P.; Cross, J. B.; Bakken, V.; Adamo, C.; Jaramillo, J.; Gomperts, R.; Stratmann, R. E.; Yazyev, O.; Austin, A. J.; Cammi, R.; Pomelli, C.; Ochterski, J. W.; Ayala, P. Y.; Morokuma, K.; Voth, G. A.; Salvador, P.; Dannenberg, J. J.; Zakrzewski, V. G.; Dapprich, S.; Daniels, A. D.; Strain, M. C.; Farkas, O.; Malick, D. K.; Rabuck, A. D.; Raghavachari, K.; Foresman, J. B.; Ortiz, J. V.; Cui, Q.; Baboul, A. G.; Clifford, S.; Cioslowski, J.; Stefanov, B. B.; Liu, G.; Liashenko, A.; Piskorz, P.; Komaromi, I.; Martin, R. L.; Fox, D. J.; Keith, T.; Al-Laham, M. A.; Peng, C. Y.; Nanayakkara, A.; Challacombe, M.; Gill, P. M. W.; Johnson, B.; Chen, W.; Wong, M. W.; Gonzalez, C.; Pople, J. A. *Gaussian 03*, revision D.02; Gaussian, Inc.: Wallingford, CT, 2004.
(54) (a) Miskowski, V. M.; Houlding, V. H. *Inorg. Chem.* **1991**, *30*, 4446. (b) Marino, N.; Fazen, C. H.; Blakemore, J. D.; Incarvito, C. D.; Hazari, N.; Doyle, R. P. *Inorg. Chem.* **2011**, *50*, 2507.